

Electron injection model for linear and parabolic 2D materials: Full quantum time-dependent simulation of graphene devices

Zhen Zhan^{1,2}, Enrique Colomés², Devashish Pandey², Shengjun Yuan¹ and
Xavier Oriols²

¹ School of Physics and Technology, Wuhan University, Wuhan 430072, China.

² Departament d'Enginyeria Electrònica, Universitat Autònoma de Barcelona, Spain.

E-mail: xavier.oriols@uab.es

1 May 2022

Abstract. The simulation of electronic devices always implies a partition between an open system and its environment. The environment fixes the conditions at the borders of the open system through local and non-local thermodynamic arguments. For time dependent simulations, such boundary conditions determine how and when electrons are injected into the open system. In this paper, the electron injection model for, both, parabolic and linear band two-dimensional (2D) materials is presented. The relevant differences between the two injection models and its implications on the device performances are indicated. In devices with gapless materials like graphene, the injection of electrons with positive and negative kinetic energies are needed for an accurate description of the band-to-band Klein tunneling. Then, the number of injected electrons is bias-dependent, implying that an extra charge is required to properly compute the device electrostatics. In addition, the injection rate in linear band materials (with an energy-independent electron velocity) tends to be a constant value, while it has a large dispersion of values in parabolic band materials (with energy-dependent electron velocities). Numerical results with the BITLLES simulator are presented showing the successful application of the electron injection model for a full quantum treatment of DC, AC, transient and noise behaviors of 2D devices.

Keywords: Electron injection model, Graphene, Klein tunneling, Additional charge, Quantum mechanics

1. Introduction

The ITRS [1] and the IRDS [2] report that electron devices are entering into the nanoscale era with TeraHertz frequencies and nanometric gate lengths [3]. In such operating conditions, the required device performance is difficult to achieve because of the short-channel problems, parasitic effects, etc. [4–7]. New 2D materials, such as graphene and transition metal dichalcogenides (MoS_2 , WS_2 and so on), are being investigated to avoid/minimize these difficulties [8–10]. The accurate modeling of 2D transistors is not trivial because some novel physical phenomena, like Klein tunneling or electrons with positive and negative kinetic energies, need to be properly tackled [11–14].

All electron device simulators split the whole device into the open system and the environment. From a computational point of view, the open system is defined as the simulation box that includes, at least, the device active region. The environment determines the boundary conditions at the borders of the simulation box through thermodynamical arguments [15, 16]. In principle, the dynamics of the relevant degrees of freedom in the open system (the transport electrons) are described from mechanical (classical [17, 18] or quantum [19–21]) equations of motion. An important part of the boundary conditions at the contacts are the so-called electron injection models. In particular, in this paper, we discuss the electron injection model for linear band (like graphene) or parabolic band (like black phosphorus) 2D materials.

In general, there are strong practical arguments in favor of using time-independent approaches for device simulation since they have less computational burden. In such time-independent models, the electron injection model basically reduces to a discussion on the density of states and the occupation function at the borders. However, time-independent approaches have difficulties to properly describe properties related to the dynamics of electrons (such as transient and AC performances [15, 22]) or to the stochastic and discrete nature of electrons (such as shot and thermal noise [20, 23]).

The time-dependent electron injection model explained here can be applied to semi-classical or quantum simulators. For semi-classical modeling [17, 18], electrons are described as point-particles, while for quantum modeling, the wave nature of electrons is accounted by time-dependent wave packets [19]. In fact, the practical examples explained in this paper are obtained from the full quantum Monte Carlo time-dependent BITLLES [24] simulator where the wave nature of electrons is described by a bispinor solution of the Dirac equation, while their particle nature by quantum (bohmian) trajectories [24–32].

After this brief introduction, the local and non-

local properties that determine the time-dependent electron injection model for parabolic and linear band structures are explained in section 2 and section 3, respectively. A comparison of linear and parabolic 2D injection models is done in section 4, together with numerical results for a graphene transistor. Finally, we conclude this paper in section 5, indicating which relevant differences on the performances of electron devices with the linear or parabolic band materials can be expected.

2. Local conditions of the injection model

In this section, we will discuss those spatial local (depending on the properties of only one contact, not both) effects that are relevant for defining an electron injection model.

There is no unique local argument to define a time-dependent electron injection model. For example, when the boundary conditions are defined far from the device active region (for large simulation boxes), it is reasonable to assume that the electron injection model has to satisfy charge neutrality. This local condition in the physical (real) space determines how many electrons need to be injected at each time step of the whole simulation. However, in positions closer to the device active region (for small simulation boxes) charge neutrality is not fully justified. Then, it is assumed that electrons entering into the simulation box are in thermodynamic equilibrium (with an energy distribution determined by a Fermi-Dirac function) with the rest of electrons in the contact [33]. The thermodynamic equilibrium in this second model is basically imposed on electrons entering into the simulation box, not on those leaving it. In this letter, this second model is adapted to 2D materials.

2.1. Density of electrons in the phase-space

The position of electrons in a 2D material is defined with the 2D vector $\{x, z\}$ (for a quantum description of the electrons, the values can be assigned to the central position of the wave packet). Electron transport (from source to drain) takes place in the x direction. Then, we define a phase-space cell, labeled by the position $\{x_0, z_0\}$ and wave vector $\{k_{x0}, k_{z0}\}$ with a volume $\Delta x \Delta z \Delta k_x \Delta k_z$, as the degrees of freedom $\{x_0, z_0, k_x, k_z\}$ satisfying $x_0 < x < x_0 + \Delta x$, $z_0 < z < z_0 + \Delta z$, $k_{x0} < k_x < k_{x0} + \Delta k_x$ and $k_{z0} < k_z < k_{z0} + \Delta k_z$. As a consequence of the Pauli exclusion principle [33], the maximum number of available electrons n_{2D} in this phase-space cell in the contact borders is:

$$n_{2D} = g_s g_v \frac{\Delta x \Delta z \Delta k_x \Delta k_z}{(2\pi)^2} \quad (1)$$

where the g_s and g_v are the spin and valley degeneracies, respectively. See Appendix A in the supplemental material to specify the physical meaning of Δx , Δz , Δk_x , Δk_z in terms of the wave packet nature of (fermions) electrons with exchange interaction. Eq. (1) specifies that, in average, each electron requires at least a partial volume 2π for each *position* \times *wave vector* product of the phase space. Each electron requires a volume $(2\pi)^2$ of the whole available phase space in a 2D material.

2.2. Minimum temporal separation t_0 between electrons

At any particular time t , all electrons with wave vector $k_x \in [k_{x0}, k_{x0} + \Delta k_x]$ inside the phase cell will attempt to enter into the simulation box during the time-interval Δt . We define $\Delta t = \Delta x/v_x$ as the time needed for the electrons with velocity component in the transport direction v_x to move a distance Δx . The time-step Δt is always positive, because electrons entering from the right contact with negative velocity move through a distance $-\Delta x$. Notice that we have assumed that the phase space cell is so narrow in the wave vector directions that all electrons have roughly the same velocity v_x . Therefore, the minimum temporal separation, t_0 between injected electrons from that cell, defined as the time step between the injection of two consecutive electrons into the system from the phase space cell, can be computed as the time-interval Δt divided by the number of available carriers n_{2D} in the phase-space cell:

$$t_0 = \frac{\Delta t}{n_{2D}} = \frac{(2\pi)^2}{g_s g_v} \frac{1}{v_x \Delta z \Delta k_x \Delta k_z} \quad (2)$$

As we have mentioned above, the injection model described here is valid for either classical or quantum systems. For a quantum system, electrons are described by wave packets. Such wave packets in the contacts can be expected to be defined by wave functions, like Gaussian wave packets or Gaussian bispinors, where a meaningful definition of its mean (central) position and wave vector is given.

For materials with a parabolic band structure, the velocity in the transport direction is $v_x^p = \frac{1}{\hbar} \frac{\partial E^p}{\partial k_x} = \frac{\hbar k_x}{m^*}$, m^* being the electron effective mass. Substituting v_x^p into equation (2) we obtain:

$$t_0^p = \frac{(2\pi)^2}{g_s g_v} \frac{m^*}{\hbar k_x \Delta z \Delta k_x \Delta k_z} \quad (3)$$

From equation (3), it is clear that the t_0 is only affected by the wave vector k_x , and for instance an electron with higher k_x needs less injection time t_0 to enter in the system.

For materials with a linear band structure, the velocity of electrons in the transport direction is $v_x^l =$

$sv_f k_x / |\vec{k}|$, s being the band index and v_f the Fermi velocity. It is important to emphasize that the x component electron velocity v_x^l is explicitly dependent on both wave vector components k_x and k_z , which is different from the v_x^p whose velocity is only determined by k_x . Then the minimum temporal separation is written as:

$$t_0^l = \frac{(2\pi)^2}{g_s g_v} \frac{|\vec{k}|}{sv_f k_x \Delta z \Delta k_x \Delta k_z} \quad (4)$$

According to (4), the temporal separation between two electrons with smaller k_z will be shorter than that with a larger k_z . As a consequence, almost all electrons in graphene are injected with a low k_z (with $k_x \approx |\vec{k}|$) and with a velocity close to the maximum value, i.e. $v_x \approx v_f$.

2.3. Thermodynamic equilibrium

We assume that electrons inside the contacts are in thermodynamic equilibrium. For electrons (fermions), the Fermi-Dirac distribution $f(E)$ provides the probability that a quantum state with energy E is occupied:

$$f(E) = \frac{1}{\exp[(E - E_f)/(k_B T)] + 1} \quad (5)$$

where E_f is the quasi Fermi level (chemical potential) at the contact, k_B is the Boltzmann constant and T is the temperature. The electron energy E is related to its wave vector by the appropriate linear or parabolic energy dispersion. We notice that the assumption of thermodynamic equilibrium is an approximation because the battery drives the electron device outside of thermodynamic equilibrium (this approximation explains why we define a quasi-Fermi level, not an exact Fermi level). We notice that there is no need to anticipate the energy distribution or electrons leaving the simulation box (the equations of motion of electrons implemented inside the simulation box will determine when and how electrons leave the open system).

2.4. Probability of injecting N electrons during the time interval τ

At temperature $T = 0$, the mean number of electrons in the phase-space cell $q(N)$ is equal to $\langle N \rangle \equiv n_{2D}$ given by (1), which means that electrons are injected regularly at each time interval t_0 . At higher temperature $T > 0$, the mean number of electrons in the cell $\langle N \rangle$ is lower than n_{2D} . In fact, because of (5), we get $\langle N \rangle \equiv n_{2D} \cdot f(E)$. The statistical charge assigned to this cell is therefore equal to $\langle Q_{2D} \rangle \equiv -q \cdot n_{2D} \cdot f(E)$. Here q is the elementary charge without sign. The physical meaning of $\langle N \rangle \equiv n_{2D} \cdot f(E)$

is that the number of electrons N in the cell (all with charge $-q$) varies with time. We cannot know the exact number N of electrons at each particular time, but statistical arguments allow us to determine the probabilities of states with different N . Such randomness in N implies a randomness in the number of electrons injected from each cell. This temperature-dependent randomness is the origin of the thermal noise [33,34].

It is known that the injection processes follow the Binomial distribution with a probability $Prob(E)$ [33]. For example, for the local conditions discussed in this section we can assume that the probability of effectively injecting electrons with energy E is given by the Fermi-Dirac statistics discussed in (5), i.e. $Prob(E) \equiv f(E)$. The probability $P^i(N, \tau)$ that N electrons are effectively injected into a particular cell i adjacent to the contact during a time-interval τ is defined as:

$$P^i(N, \tau) = \frac{M_\tau!}{N!(M_\tau - N)!} Prob(E)^N (1 - Prob(E))^{M_\tau - N} \quad (6)$$

where M_τ is the number of attempts of injecting carriers in a time-interval τ , defined as a number we get by rounding off the quotient τ/t_0 to the nearest integer number towards zero, i.e. $M_\tau = \text{floor}(\tau/t_0)$. The number of injected electrons is $N = 1, 2, \dots, M_\tau$.

3. Non-local conditions of the injection model

We now discuss some non-trivial non-local effects that have to be considered in the practical development of an electron injection model for 2D materials.

3.1. Transport, non-transport electrons and holes in parabolic bands

In order to simplify the computations, not all electrons present in an open system are explicitly simulated. Only transport electrons, defined as those electrons whose movements are relevant for the computation of the current, are explicitly simulated. The contribution of the non-transport electrons to the current is negligible and their charge is included as part of a fixed charge. What determines if an electron is a transport electron or not? In principle, one erroneously argues that the quasi-Fermi level provides a local rule to determine if an electron is a transport electron or not. Those electrons with energies close to the quasi-Fermi level are transport electrons, while those electrons with energies well below are irrelevant for transport. This local rule is not always valid for all materials and scenarios.

When modeling traditional semiconductor devices usually the applied bias in the edges of the active region

is less than the energy band gap. See figure 1(a) and (b). Then, one can assume that transport electrons belong to just one band along the whole device, either the valence or the conduction band. Then, one can consider, for example, that all electrons in the CB are transport electrons. Electrons in the VB do not participate in the transport because there are no free states available. See blue regions for transport electrons in CB and orange region in the VB of figure 1(a) and (b). The important point is that the number of transport electrons in this case is bias independent, meaning that the number of transport electrons remains the same in figure 1(a) and (b). The division between transport and non-transport electrons in scenarios such as figure 1(c), which could correspond to a Zener diode [35] where a very large bias (greater than the energy gap) is applied, cannot be treated in the same way as the previous scenarios. Instead, this case which occurs rarely in devices with parabolic bands and large energy gap, should be treated as we treat gapless materials below.

The distinction between transport and non-transport electrons does also apply when the quasi-Fermi level is close to electrons in the VB. Then, there is no transport of electrons in the CB because there are no electrons there. We can consider as transport electrons, for example, those electrons in the valence band whose energy is no lower than $\alpha k_B T$ (generally, it is sufficient to define $\alpha = 5$) below the quasi-Fermi level at the contact. The rest of electrons in the VB with energies lower than $E_f - 5k_B T$ are non-transport electrons. In order to simplify the computational burden of transport electrons in the VB, traditionally, one simulates the absence of electrons in the VB, defined as holes, instead of the transport electrons themselves. The total current I can be computed by summing the current I_i of each transport electron in the VB, $I = \sum_{i=1}^n I_i$, where n is the number of transport electrons in the VB (with positive and negative velocities). However, if n is quite close to maximum number of allowed electrons in that region n_{max} , then, by knowing that a VB full of electrons (equal number of electrons with positive and negative energies) does not have net transport. i.e. $I_{max} = \sum_{i=1}^{n_{max}} I_i = 0$, we get:

$$I = \sum_{i=1}^n I_i - \sum_{i=1}^{n_{max}} I_i = \sum_{j=1}^{n_{max}-n} (-I_j). \quad (7)$$

Thus, instead of simulating $i = 1, \dots, n$ transport electrons we can simulate $j = 1, \dots, n'$ transport holes with $n' \equiv n_{max} - n$, assuming that the current of the holes ($-I_j$) is the opposite of the electron current I_i . This can be achieved by considering that holes have positive charge $+q$.

Let us define the fixed charge (belonging to

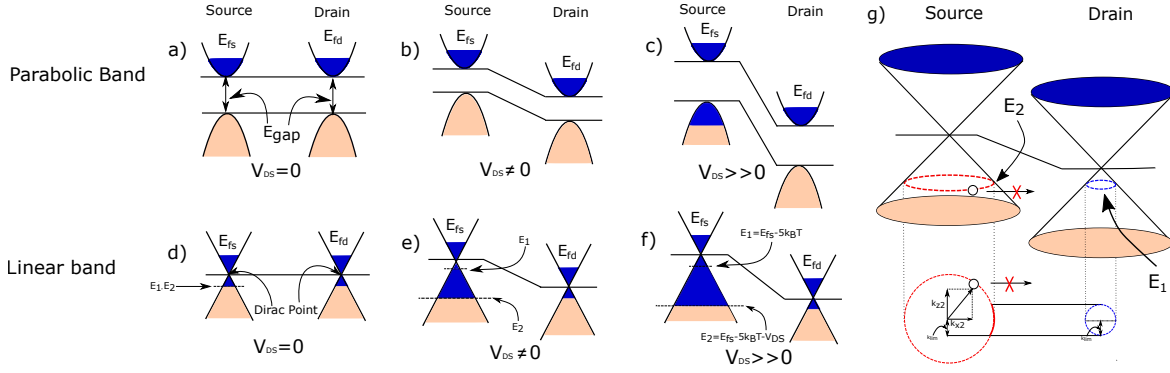


Figure 1: The energy profile for a device with parabolic CB and VB separated by an energy bandgap E_{gap} and for a gapless material with linear CB and VB where blue electrons and orange electrons are transport and non-transport ones, respectively. In the insets (a) and (b), the selection of transport and non-transport electrons is independent of the bias (same number of electrons are simulated that contribute to transport). The inset (c) corresponds to the energy profile of a Zener diode under a high reverse bias where additional transport electrons in the VB have to be considered. The insets (d), (e) and (f) corresponds to a gapless structure, where the number of transport electrons is bias dependent. The electrons in the energy range from $E_1 = E_{fs} - 5k_B T$ to $E_2 = E_{fs} - 5k_B T - V_{DS}$ are the additional transport electrons that have to be added at each bias point. (g) Representation of an electron traveling from the source to the drain. Only the electrons with the momentum range spanned by the smaller blue circle can reach the drain contact due to the conservation of k_z .

dopants or non-transport electrons below $E = E_f - 5k_B T$ in the VB as Q_{fix} . Then, the computation of the charge in the VB of parabolic materials can be also done using electrons or holes. We define $Q_{max} = \sum_{i=1}^{n_{max}} (-q_i)$ as the charge belonging to transport electrons when the energy region above $E = E_f - 5k_B T$ is full of electrons. Therefore the charge due to the n electrons in that energy region when considering the transport of holes, is:

$$Q = Q_{fix} + \sum_{i=1}^n (-q_i) = Q_{fix} + Q_{max} + \sum_{j=1}^{n'} q_j \quad (8)$$

We have to consider the holes as carriers with positive charge $+q$ and consider a fixed charge Q_{max} , in addition to Q_{fix} , when dealing with device electrostatics through the n' holes. The use of holes can be useful in scenarios like the ones in figure 1(a) and (b), when it is true that $n' \ll n$ along the whole simulation box.

The problem with the simulation of holes (instead of transport electrons) in the VB appears when electrons move from the VB to the CB in a band-to-band-tunneling process. Then, there are regions of the simulation box with more holes than other regions, see figure 1(c). Within the language of holes, such electron transit from VB to CB can be modeled as an electron-hole generation process inside the device [12]. During the transition of the electron from the VB to the CB, we can assume that an electron is effectively created in the CB, while a hole is also effectively created (an electron

disappears) in the VB. Such transition probability depends on the number of electrons (number of holes) in a particular region of the phase space inside the device, which in turn depends on the occupation probability. What is the occupation probability $f(E)$ inside the device? A fundamental simulation wants a mechanical description of the electrons inside the device, not a statistical one. Therefore, no *a priori* assumption about the occupation function inside the device is accessible in such simulations. Obviously, we can assume some thermodynamic quasi-equilibrium occupation function in these regions of the phase space inside the device. The use of holes implies an important reduction of the computational burden, at the price of reducing the fundamental character of the simulation [12,36]. The difficulties of using holes are even worst in time-dependent quantum transport because electron-hole generation would require the ad-hoc definition of the wave nature of electrons and holes in the middle of the simulation box.

3.2. Transport, non-transport electrons and holes in linear bands

The utility of the holes and the uniformity of Q_{fix} has to be revisited when dealing with linear band materials (as well as in parabolic band structure materials when the applied bias is greater than the energy bandgap as discussed in figure 1(c)) because the transition from VB to CB is unavoidable.

In figure 1(d)-(f), we see those electrons depicted in blue (dark gray) whose energy is well below the

local quasi-Fermi level in the source E_{fs} , but that effectively contribute to current because such electrons in the VB in the source contact with negative kinetic energy are able to travel through the device, cross the Dirac point via Klein tunneling and arrive at the CB with positive kinetic energy in the drain contact. We define the zero of total energy at the Dirac point. The same scenario for parabolic bands is depicted in figure 1(c). The argument saying that the VB is full of electrons in the source giving zero current ($I_{max} = \sum_{i=1}^{n_{max}} I_i = 0$) is false here. Such argument is a local argument that does not take into account the non-local relation between the source and the drain contacts. How many transport electrons contribute to the current in figure 1(d)-(f)? We have seen that electrons with energies above $E = E_{fd} - 5k_B T$ in the drain are relevant for the transport. In addition, electrons with energies below $E = E_{fs} - 5k_B T$ in the source are also relevant for transport. In order to minimize the number of transport electrons in the simulating box, we use the following algorithm. In the source contact, the transport electrons are all electrons within the energies in the range $[E_{fd} - 5k_B T, E_{fs} + 5k_B T]$ defined in figure 1(d)-(f), while the energy range $[E_{fd} - 5k_B T, E_{fd} + 5k_B T]$ is used for the drain. Since we can consider that $E_{fs} = E_{fd} + V_{DS}$ with V_{DS} the applied voltage, the number of transport electrons selected with the overall criteria is bias-dependent and position-dependent. Other criteria are also possible in the selection of the transport electrons †. The criteria specified here to select the transport electrons as explained in figure 1(d)-(f) is the one that minimizes the overall number of transport electrons.

The simulation of holes (instead of electrons) in the VB of graphene is also possible. However, there are two important difficulties. First, as discussed at the end of section 3.1, the electron-hole generation to describe the band-to-band Klein tunneling would require some type of estimation for the thermodynamic quasi-equilibrium distribution of holes inside the simulation box [12]. Second, such probability would require an ad-hoc definition of Klein tunneling transmission coefficient. However, Klein tunneling is a pure quantum interference phenomena depending on several factors (energy, direction of propagation, potential profile, etc.) implying important difficulties when attempting to develop ad-hoc analytic expressions of the Klein tunneling transmission probability §. None of the

† We notice that considering more or less transport electrons in the simulation is not a physical problem, but a computational problem because it increases the computational effort

§ For a full quantum time-dependent electron transport simulator, such electron-hole generation would require a definition of the electron and hole wave packets in the middle of the simulation box. We can assume a Gaussian type for the

above two important difficulties (definition of the occupation function inside the simulation box and the definition of an ad-hoc Klein tunneling transmission probability) are present when only transport electrons, not holes, are considered in the VB and simulated through the Dirac equation as we will shown in section 4.2.

From figure 1(e), we can rewrite the charge assigned to electrons in the CB and VB of the drain contacts for a gapless material as follows:

$$Q_{drain} = Q_{fix} + \sum_{i=1}^{n_{drain}} (-q_i) \quad (9)$$

The charge distribution in the source is not exactly the same as in (9) because, as discussed above, the number of transport electrons in the source n_{source} is different from n_{drain} . Therefore, we get:

$$Q_{source} = Q_{fix} + \sum_{i=1}^{n_{source}} (-q_i) - Q_{add}(x_{source}) \quad (10)$$

where $Q_{add}(x_{source})$ is just the additional charge assigned to the additional number of transport electrons $n_{source} - n_{drain}$ simulated in the source. In fact, as we will discuss at the end of section 3.3, in each point of the device, and each bias point, we have to consider a different value of $Q_{add}(x)$. In particular, we notice that (9) can be written as (10) with the condition $Q_{add}(x_{drain}) = 0$. Finally, we notice again that the consideration of this position dependent charge can be avoided by just using the same number of transport electrons in the drain and in the source, but this would imply an increment of the computational effort to transport electrons that, in fact, do not provide any contribution to the current. In conclusion, minimizing the number of transport electrons implies a positions and bias dependent definition of $Q_{add}(x)$.

3.3. Pauli principle between the source and drain contacts and conservation laws

We can invoke a new strategy to further minimize the number of transport electrons in the simulation box, by taking into account the Pauli exclusion principle between source and drain contacts. This strategy is based on the following two assumptions. First, we consider that electrons move quasi-ballistically inside the simulation box, so that we can reasonably predict what is the energy of an electron at the drain, initially injected from the source, and vice-versa. The second assumption is that the occupation functions at the drain and source do not only provide the energy distributions of electrons entering into the simulation

wave packet at the borders of the simulation box, however, the type of wave packet generated in the middle of the simulation box, while doing Klein tunneling, is hardly anticipated by ad-hoc models.

box, but also provide a reasonable prediction of the energy distribution of electrons leaving it. Under these two assumptions, we can avoid the injection of electrons from one side that will not be able to arrive to the other side in a later time because other electrons are occupying that region of the phase-space (positions and wave vectors). Let us notice that this new strategy can be avoided if the many body Pauli exclusion principle could be included somehow into the equation of motion of electrons inside the simulation box [19, 37].

Let us assume an electron moving *ballistically* inside the graphene channel with total energy E satisfying the energy conservation law. Assume an electron with energy E is effectively injected from the source contact, the probability that it will arrive to the drain (in thermal equilibrium) with the same energy E is given by the probability that such region of the phase space is empty of electrons, which is $f_{sd}(E) = (1 - f(E))$ with $f(E)$ given by (5) and $E_f \equiv E_{fd}$ indicating the quasi-Fermi level at the drain contact.

A similar argument can be invoked for momentum conservation. When considering transport electrons incident on a potential barrier that is translationally invariant in the z direction (perpendicular to the transport direction), i.e. $V(x, z) = V(x)$, in addition to the conservation of electron energy E , the conservation of the momentum projection k_z can also be invoked. Let us give an example on how the conservation of momentum projection k_z affects our injection model in graphene. We consider one electron with energy E injected successfully from the source contact into the system and that the electron is transmitted (without being scattered) through a potential barrier and finally arriving at the drain contact. According to the linear dispersion relation in graphene, the maximum absolute value of momentum projection k_z that the electron can obtain is $k_{lim} = |(E + qV_{DS})/(\hbar v_f)|$, see the definition of k_{lim} in figure 1(g). In the source, all those electrons whose $|k_z| > k_{lim}$ will not be able to reach the drain, i.e. only electrons whose k_z belongs to the momentum range spanned by the smaller blue circle could reach the drain. Therefore, at the source contact, the probability P_{k_z} that an injected electron will satisfy the conservation of momentum is given by:

$$P_{k_z} = \left(1 - \Theta(|k_z| - k_{lim})\right) \quad (11)$$

where $\Theta(|k_z| - k_{lim})$ is a Heaviside step function.

Up to now, we have mentioned three (one local and two non local) conditions to determine the probability that an electron is effectively injected from the source. At the source contact, the probability $f_{sum}(E)$ that the electron is effectively injected from the source as a

transport electron is:

$$\begin{aligned} f_{sum}(E) &= f_s(E) f_{sd}(E) P_{k_z} \\ &= \frac{1}{\exp[(E - E_{fs})/(k_B T)] + 1} \\ &\times \left(1 - \frac{1}{\exp[(E - E_{fd})/(k_B T)] + 1}\right) \\ &\times \left(1 - \Theta(|k_z| - k_{lim})\right) \end{aligned} \quad (12)$$

The Fermi-Dirac distribution in (5) is a general law used in most nanoscale simulators. The other two additional laws are optional requirements of the injection model that allow a reasonable reduction of the simulated number of transport electrons without affecting the current computations, which could be eliminated if a many body treatment of the equation of motion of electrons is present in the simulation box. However, in traditional single-particle treatment of the equation of motion, such requirements tend to capture the role of the Pauli exclusion principle in the dynamics of the electrons inside the simulation box.

The figure 2 illustrates how the additional two laws (non-local conditions) affect the energy distribution in the new injection model in the case of injected electrons having ballistic transport in graphene transistors. In figure 2(a), all the electrons in VB are attempted to be injected into the system. However, in figure 2(b), when the non-local conditions are included, the energy distribution in VB is different from that in figure 2(a). In figure 2(b), less electrons from VB attempt to be injected into the system with an important reduction of the number of injected electrons, which in case of being injected would not contribute to transport properties. The occupation probability for the electrons in VB with $k_z > 0.5 \text{ nm}^{-1}$ equals to 0, which is a result of the k_z conservation. The probability for the electrons in VB with energy $E > 0.2 \text{ eV}$ (for $|\vec{k}| > 0.5 \text{ nm}^{-1}$) approximates to 0, which is a result of the correlation between the source and drain contacts.

Finally, let us exemplify how we introduce the additional charge in (9) and (10) in a graphene device. Our purpose here is to compute the charge of electrons that will be injected in a non equilibrium scenario, but not injected in the equilibrium scenario (figure 1(c)). The density of states in 2D linear graphene is:

$$D_{gr}(E) = \frac{g_s g_v |E|}{2\pi \hbar^2 v_f^2} \quad (13)$$

where the spin degeneracy $g_s = 2$ and the valley degeneracy $g_v = 2$. Regarding figure 1(f), in principle the amount of charge Q_{add} would be computed from the integral of $D_{gr}(E)$ from E_2 to E_1 . However,

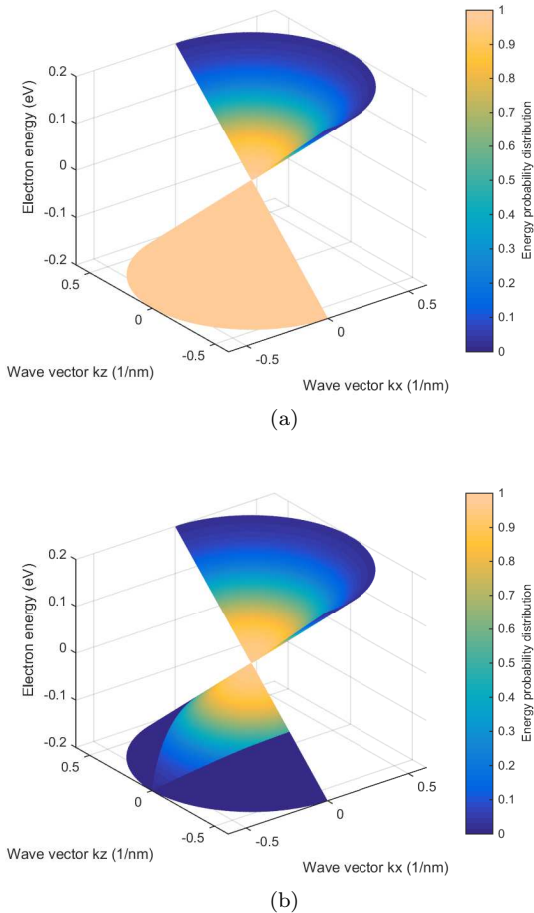


Figure 2: The energy distribution of the electrons with positive (in CB) and negative energies injected from the source contact plotted in (a) which is computed from equation (5) and in (b) which is computed from equation (12). The absolute temperature $T = 300$ K, Fermi-level at the source contact $E_{fs} = 0.1$ eV, an voltage drop $V_{DS} = 0.3$ V applied to the device and the Fermi velocity $v_f = 5 \times 10^5$ m/s.

this is not fully true. Firstly, only electrons going in the transport direction are simulated, so we just need half of this charge. In addition, as presented above we also have to account for the conservation of momentum k_z for all energy levels from E_2 until E_1 . For that reason, for example not all electrons from the energy level E_2 will be able to arrive to the drain, and just a fraction of them will be injected. This fraction is easily understood from figure 1(g). Only electrons belonging to the circumference arc will be injected and will be able to reach the drain. The semi-circumference length is $L = \pi E_2$ and the length of the mentioned circumference arc is $L_a = 2|E_2| \arcsin(E_1/E_2)$. Therefore, the ratio to be injected is $L_a/L = 2 \arcsin(E_1/E_2)/\pi$. This calculus must be performed along the device. Then, the amount

of charge to be added (Q_{add}) in each point of the device is the following:

$$Q_{add}(x) = q \int_{E_{fs} - 5k_B T - V_{DS}}^{E_{fs} - 5k_B T - V(x)} \frac{g_s g_v |E|}{2\pi \hbar^2 v_f^2} F_{corr} dE \quad (14)$$

where F_{corr} is the correction factor and is equal to $F_{corr} = L_a/2L$. The technical details about the implementation of the injection model in the BITLLES simulator is explained in the Appendix B of the supplemental material.

4. Numerical results

In section 4.1, we provide a discussion on how the local conditions studied in section 2 provide some important differences in the injection from linear or parabolic 2D materials. Then, in section 4.2, we will discuss the results of the local and non-local conditions on the electron injection model described in this paper when applied to graphene transistors.

4.1. Local conditions on the electron injection from parabolic or linear 2D materials

The effect of the material energy spectrum on the number of attempts of injecting electrons into the system is plotted in figure 3. As it can be seen in figure 3(b), only electrons with large k_x are injected into the system. However, in the case of materials with linear dispersion relations, as shown in figure 3(a), the majority of injected electrons have smaller k_z . As a consequence, most injected electrons move in the transport direction at the saturation velocity $v_x \approx v_f$ (with $|k_x| \approx |\vec{k}|$).

This difference in the type of injection can imply relevant differences between the electrical properties of electrons devices fabricated with 2D materials with linear or parabolic bands. As a simple estimation, we assume a ballistic transport in the electronic device and compute the (instantaneous) total current I from each electron inside the simulation box. The current I is computed by using the (Ramo-Shockley-Pellegrini) expression $I = qv_x/L_x$, L_x being the source-drain distance. As plotted in figure 4(a), almost all electrons injected from a contact with linear band structure have the same velocity and carry the same instantaneous current I . On the contrary, in figure 4(b), electrons injected from a parabolic band structure material has large dispersion in both the velocity and instantaneous current I . The current dispersion (noise) of both types of band structures are dramatically different, which can have relevant effects in the intrinsic behaviour of AC and noise performances.

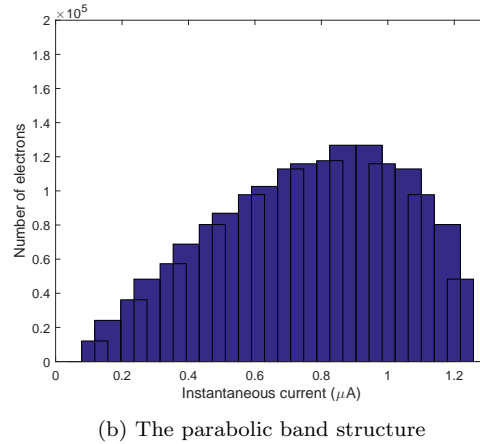
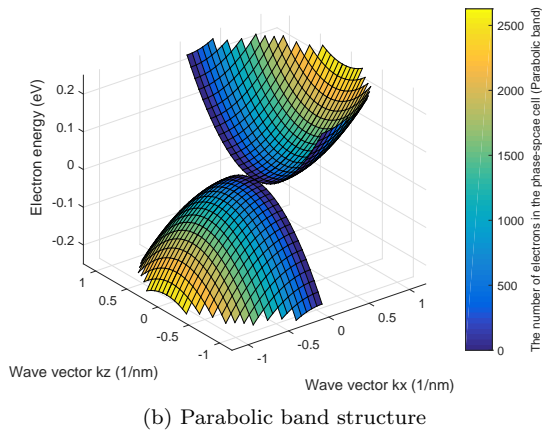
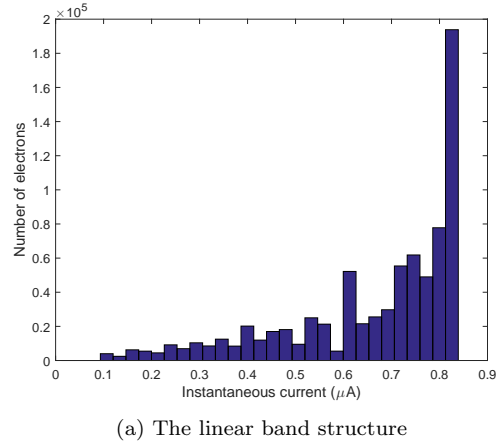
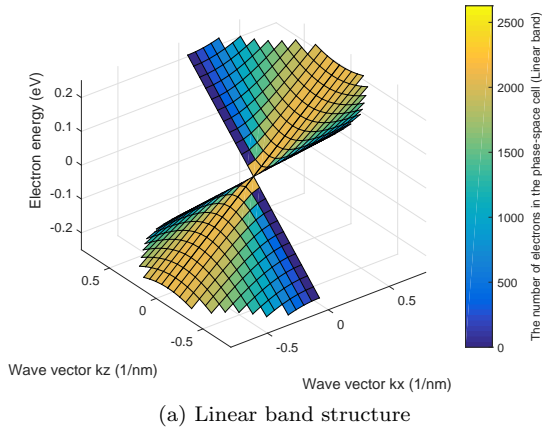


Figure 3: Number of attempts of injecting electrons computed from equation (4) plotted in (a) and from equation (3) in (b) for a cell $\Delta x \Delta z \Delta k_x \Delta k_z$ during a simulation time $\Delta t = 0.1$ ns at zero temperature. The parameter $m^* = 0.2m_0$ being m_0 the free electron mass, $g_s = 2$, $g_v = 2$, fermi velocity $v_f = 5 \times 10^5$ m/s, the dimensions of the phase-space cell are selected as $\Delta x = \Delta z = 1 \times 10^{-7}$ m, $\Delta k_x = \Delta k_z = 3 \times 10^7$ m $^{-1}$.

4.2. Simulation of graphene transistors

We present numerical results for two different graphene transistors (GFET) performed with the BITLLES simulator following the injection model presented here including the additional charge. Electrons injected are described by conditional Gaussian wave packets, following Fermi statistics at room temperature. Then, all pseudo Dirac equations \parallel (one for each injected electron) are coupled to the Poisson equation and solved self-consistently (for additional information see Refs. [19,32,38]).

\parallel Details about how the Dirac equation is solved are explained in the Appendix C of the supplemental material.

Figure 4: Number of electrons as a function of instantaneous current I for materials with (a) a linear and (b) a parabolic band structure during $\tau = 0.1$ ns at zero temperature. The simulation conditions are the same as in figure 3 and with Fermi level $E_f = 0.32$ eV.

Current-voltage characteristic The first GFET simulated has the following parameters: channel length is $L_x = 40$ nm, width $L_z = 250$ nm and Fermi energy is 0.15 eV above the Dirac point. It has bottom and top gates, whose voltages are set equal to zero, $V_{bg} = V_{tg} = 0$ V. In figure 5, we see two different current-voltage characteristics of a ballistic GFET. The insets are related to the one plotted in figure 1 indicating the relevant presence of electrons with energy above the Dirac point (CB), and below (VB). The solid curve corresponds to the scenario where electrons are injected from both CB and VB. Contrary to normal FETs, there is no saturation current, since the more the voltage is applied between source and drain, the more number of electrons are transmitted from the source to the drain (from valence band in the source to conduction band in the drain). On the other hand, in the dashed curve, we allow only injection from the

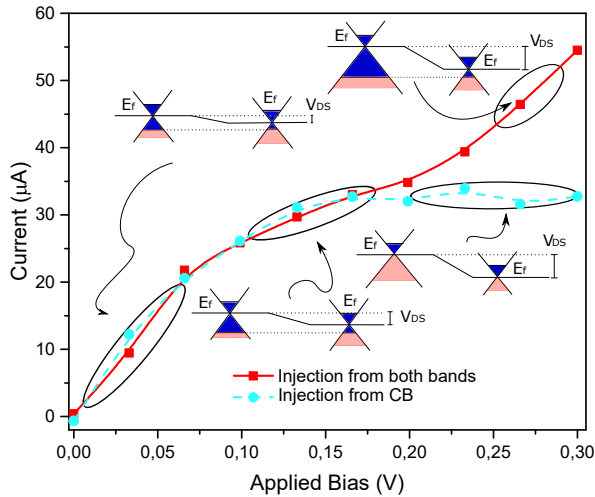


Figure 5: Current-voltage characteristic for the GFET. The red solid (square) line corresponds to normal graphene injection (electrons injected from both the CB and VB) current-voltage characteristic, while in the blue dashed (circle) line only electrons from the CB are injected. The insets sketch different energy profiles for applied bias.

CB. Then, current saturates because after the voltage reaches the Fermi energy value, the same amount of electrons from the conduction band are injected independently of the applied voltage. This is similar to typical FETs with semiconductors having energy gap large enough such that typically only electrons from the conduction band (or only electrons from the valence band) are considered.

Transient In this other example, we present (see figure 6) the instantaneous current after a transient perturbation in the gates. This scenario is useful to study high-frequency effects [39]. We used another GFET with the same parameters, except for the channel length, which is $L_x = 400\text{nm}$. In figure 6, we see the mean current (in solid thick lines) in the drain, source and gate as function of time, and their instantaneous current (in thin lines). After time $t = 1$ ps, the current in the drain increases, contrary to the source, that decreases after the gate voltage perturbation. We notice that the total (particle plus displacement) current has been computed for each contact. At each time step, the sum of the three currents is zero satisfying current conservation law. We see in figure 6 the transient dynamics related to the electron dwell time (with Klein tunneling) and the noise induced by the randomness in the electron injection process.

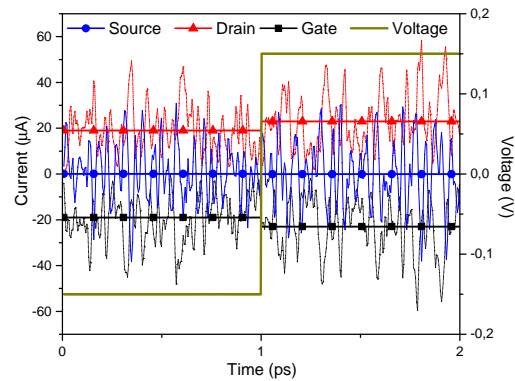


Figure 6: The transient current in a GFET. Initially both (top and bottom) gates voltage values are set to $V_{bg} = V_{tg} = -0.15$, at time $t = 1$ ps this values is changed to $V_{bg} = V_{tg} = 0.15$.

5. Conclusions

The electron injection model in linear band structure materials has some particularities not present in the traditional modeling of electron transport in bulk materials. In particular, in gapless materials like graphene with a linear band structure, the injection of electrons with positive and negative kinetic energies are needed to properly treat current-voltage characteristics with Klein tunneling. Then, it is shown that the number of injected electrons are bias dependent so that an extra charge has to be added when computing the device electrostatics. From the differences in the linear and parabolic energy bands of materials, we can anticipate some important differences in noise generated by the contacts. The injection rate in linear band materials tends to a constant value. Local and non-local constraints in the development of the injection model are discussed. Numerical results showed in section 4 validates the correctness of the injection model of the BITLLES simulator [22, 25–31, 38] to study quantum transport for DC, AC and noise in different 2D devices, including GFETs. Future work will be devoted to the difference in the high-frequency noise between devices with parabolic and linear band structures, which will open many unexplored applicabilities of using this noise as band structure tester.

Acknowledgement

We acknowledge funding from Fondo Europeo de Desarrollo Regional (FEDER), the “Ministerio de Ciencia e Innovación” through the Spanish Project TEC2015-67462-C2-1-R, the Generalitat de Catalunya

(2014 SGR-384), the European Union's Horizon 2020 research and innovation programme under grant agreement No Graphene Core2 785219 and under the Marie Skłodowska-Curie grant agreement No 765426. Yuan acknowledges financial support from Thousand Young Talent Plan (China).

References

- [1] International Technology roadmap for semiconductors
- [2] International roadmap for device and systems
- [3] Schwierz F, Pezoldt J and Granzner R 2015 *Nanoscale* **7** 8261-8283
- [4] Schwierz F 2013 *Proc. IEEE* **101** 1567
- [5] Schwierz F 2010 *Nat. Nanotechnol.* **5** 487
- [6] Fiori G, Bonaccorso F, Iannaccone G, Palacios T, Neumaier D, Seabaugh A, Banerjee S K and Colombo L 2014 *Nat. Nanotechnol.* **9** 768
- [7] Jung H-E and Shin M 2017 *Nanotechnology* **29** 025201
- [8] Logoteta D, Fiori G and Iannaccone G 2014 *Sci. Rep.* **4** 6607
- [9] Pudasaini P R, Stanford M G, Oyedele A, Wong A T, Hoffman A N, Briggs D, Xiao K, Mandrus D G, Ward T Z and Rack P D 2017 *Nanotechnology* **28** 475202
- [10] Hur J-H and Kim D-K 2018 *Nanotechnology* **29** 185202
- [11] Katsnelson M I, Novoselov K S and Geim A K 2006 *Nat. Phys.* **2** 620-625
- [12] Paussa A, Fiori G, Palestri P, Geromel M, Esseni D, Iannaccone G and Selmi L 2014 *IEEE Trans. Electron Devices* **61** 5
- [13] Iannaccone G, Bonaccorso F, Colombo L and Fiori G 2018 *Nat. Nanotechnol.* **13** 183-191
- [14] Millithaler J-F, Iñiguez-de-la-Torre I, Mateos J, González and Margala M 2015 *Nanotechnology* **26** 485202
- [15] Frensley W R 1990 *Rev. Mod. Phys.* **62** 745
- [16] Rossi F 2011 *Theory of semiconductor quantum devices: microscopic modeling and simulation strategies* (Berlin: Springer-Verlag Berlin Heidelberg)
- [17] Jacoboni C and Reggiani L 1983 *Rev. Mod. Phys.* **55** 645700
- [18] Gonzalez T, Mateos J, Pardo D, Varani L and Reggiani L 1999 *Semicond. Sci. Technol.* **14** 3740
- [19] Oriols X 2007 *Phys. Rev. Lett.* **98** 066803
- [20] Blanter Y M and Buttiker M 2000 *Phys. Rep.* **336** 1166
- [21] Datta S. *Electronic transport in mesoscopic systems.* Cambridge, UK: Cambridge Univ. Press; 1995.
- [22] Traversa F L, Buccafurri E, Alarcón A, Albareda G, Clerc R, Calmon F, Poncet A and Oriols X 2011 *IEEE Trans. Electron Devices* **58** 2104
- [23] Büttiker M 1992 *Phys. Rev. B* **46** 12485
- [24] The BITLLES simulator is free available at: <http://europe.uab.es/bitlles>
- [25] Alarcón A, Cartoixà X and Oriols X 2010 *Phys. Status Solidi* **7** 2636-2639
- [26] Alarcón A, Yaro S, Cartoixà X and Oriols X 2013 *J. Phys. Condens. Matter* **25** 325601
- [27] Albareda G, López H, Cartoixà X, Suñé J and Oriols X 2010 *Phys. Rev. B* **82** 085301
- [28] Albareda G, Suñé J and Oriols X 2009 *Phys. Rev. B.* **79** 075315
- [29] Marian D, Colomé E and Oriols X 2015 *J. Phys. Condens. Matter* **27** 245302
- [30] Marian D, Colomé E, Zhan Z and Oriols X 2015 *J. Comp. Elect.* **14** 114
- [31] Alarcón A and Oriols X 2009 *J. Stat. Mech. Theory Exp.* **2009** 01051
- [32] Oriols X and Mompert J 2011 *Applied Bohmian Mechanics: From Nanoscale Systems to Cosmology* (Singapore: Pan Stanford Publishing)
- [33] Oriols X, Fernandez-Diaz E, Alvarez A and Alarcón A 2007 *Solid State Electron.* **51** 306
- [34] Landauer R and Martin T 1991 *Physica B* **175** 16777
- [35] Zener C M 1948 *Elasticity and anelasticity of metals* (Chicago: University of Chicago Press)
- [36] Schwierz F, Pezoldt J and Granzner R 2017 *IEEE Trans. Electron Devices* **64** 6
- [37] Oriols X 2004 *Nanotechnology* **15** 16775
- [38] Colomé E, Zhan Z, Marian D and Oriols X 2017 *Phys. Rev. B* **96** 075135
- [39] Zhan Z, Colomé E and Oriols X 2017 *IEEE Trans. Electron Devices* **64** 2617